# Submicrometer surface structuring with a Bessel beam generated by a reflective axicon

Cite as: J. Laser Appl. **33**, 042013 (2021); https://doi.org/10.2351/7.0000532
Submitted: 13 July 2021 • Accepted: 03 September 2021 • Published Online: 28 September 2021

Martin Osbild, Elisabeth-Annemarie Gerhorst, Siddharth Sivankutty, et al.

Journal of Laser Applications ARTICLE scitation.org/journal/jla

# Submicrometer surface structuring with a Bessel beam generated by a reflective axicon

Cite as: J. Laser Appl. 33, 042013 (2021); doi: 10.2351/7.0000532
Submitted: 13 July 2021 · Accepted: 3 September 2021 ·
Published Online: 28 September 2021



Martin Osbild,[1] Elisabeth-Annemarie Gerhorst,[2] Siddharth Sivankutty,[3] Gwenn Pallier,[3] and Guillaume Labroille[3]

## AFFILIATIONS

[1]Fraunhofer Institute for Laser Technology, Steinbachstr. 15, Aachen 52074, Germany
[2]Chair for Laser Technology LLT, RWTH Aachen University, Steinbachstr. 15, Aachen 52074, Germany
[3]Cailabs, 38 Boulevard Albert 1er, Rennes 35200, France

**Note:** Paper published as part of the special topic on Proceedings of the International Congress of Applications of Lasers & Electro-Optics 2021.

## ABSTRACT

In ultrashort pulse (USP) laser ablation, focus diameters in the range of >20 $\mu$m are common for microstructuring, but the demand for much smaller structure sizes is rising, especially in the fields of filter technology, surface functionalization, and electronics. However, strong focusing of a Gaussian beam near the diffraction limit is accompanied by a very limited depth of focus, which leads to an extreme increase in process sensitivity. It is often too challenging to meet the necessary precision requirements for the system technology. A potential solution to overcome the problem of the short focus depth is the usage of a nondiffracting Bessel beam that is well known for providing a depth of field in the mm range while allowing the diameter of the central processing spot to be below 1 $\mu$m. There are several ways to generate a Bessel beam, but only an axicon is suitable for efficient high-power USP ablation. However, even high-precision manufactured axicons have a round tip resulting in a highly oscillating intensity along the propagation axis. This characteristic is a major obstacle for reproducible and reliable laser nanostructuring of metals. For this reason, reflective axicons were newly introduced to the market. They generate a Bessel beam much closer to the ideal axial intensity distribution. In this paper, we compare the Bessel beam generated by a reflective axicon with that of a conventional axicon in an application-oriented setting. Furthermore, we demonstrate the enormous potential of Bessel beams for surface structuring.

Key words: Bessel beam, axicon, nanostructuring, surface structuring, ultrashort pulse laser



## I. INTRODUCTION

Bessel beams have found their niche in materials processing, whenever small processing diameters with a large depth of field are advantageous. Due to the nondiffractive properties of the Bessel beam, even spot sizes in the submicrometer range are easily achievable with an independent depth of field of several mm, whereas conventional focusing of a Gaussian beam on a 1 $\mu$m spot would result in a Rayleigh length in the low single-digit micrometer range due to the beam caustic. These extreme aspect ratios of Bessel beams were predominantly exploited in the processing of transparent material, like in glass cutting[1] or the fabrication of nanochannels in glass.[2,3] However, surface structuring of nontransparent material can also profit from the properties of a Bessel beam when small spot sizes are required. The extremely generous focal plane tolerance is particularly beneficial for rough, prestructured, and uneven surfaces or when the positioning accuracy of the machine is low.[3–5]

In the literal sense, Bessel beams are theoretical beams whose lateral electric field distribution is described by the zeroth-order Bessel function of the first kind $J_0$ containing infinite energy over an infinite size.[6] Under real conditions, spatially limited Bessel-like beams can be generated by shaping a laser beam with a Gaussian-like energy distribution, which was first discovered in 1987.[7] They are also called quasi-Bessel beams or Bessel–Gauss beams but for simplicity they will be referred to as Bessel beams in this paper. The cross section of a Bessel beam can be described as concentric interference rings with a central lobe (Bessel core) containing the highest energy density. Only

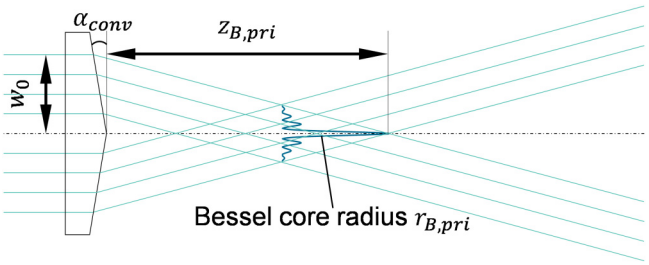


**FIG. 1.** Generation of a Bessel beam by a conventional axicon.

that part of the Bessel beam is effectively used in most material processing applications.

There are many methods how to shape a generic laser beam into a Bessel beam. The oldest method is the illumination by a collimated laser through an annular slit placed in the focal plane of a positive lens.[7] Bessel beams can also be generated by a diffractive optical element,[8–10] a spatial light modulator,[11,12] or an axicon. Axicons feature the least energy loss and the highest damage threshold among all optical components known for generating a Bessel beam. In the original sense, it is a conically ground positive glass lens invented in 1960 well before the discovery of the Bessel beam.[13] The conical surface refracts the incident plane waves toward the optical axis inducing the beam to interfere with itself (Fig. 1). This conventional type of axicon is simple to manufacture and affordable and, therefore, most widely used. A variant of the refractive axicon is the negative axicon, whose fabrication and evaluation have only been reported in the literature, though.[14]

Conventional axicons have two typical manufacturing errors that have been studied thoroughly. One of them is an elliptical cross section resulting in a nonrotational symmetric beam.[15,16] The resulting intensity pattern is often described to look like a checkerboard or four-leaf clover. The other manufacturing error is the axicon's imperfect tip.[6,17,18] The typically round tip locally acts as a convex lens, causing intensity oscillations in the Bessel core along the propagation axis.[18] This is a quality-limiting factor in volume structuring and can also significantly reduce the process stability in surface structuring. Several techniques have been developed to circumvent the effects of imperfect tips, such as Fourier filtering[6] or the use of liquid immersion.[19] However, they are neither energy efficient nor easy to implement.

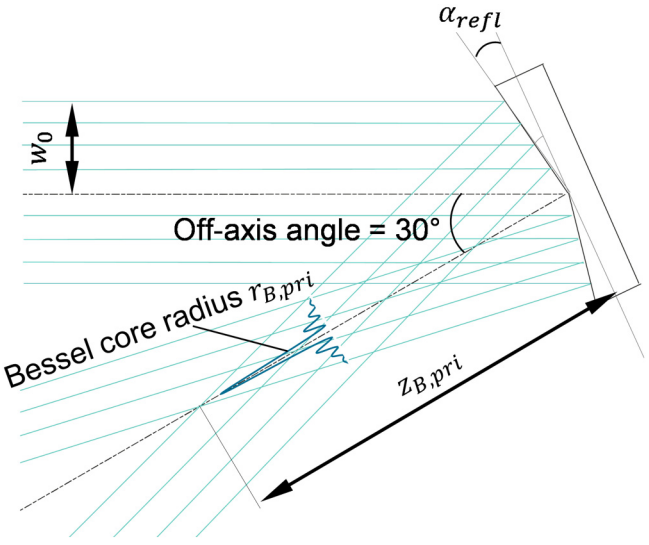


**FIG. 2.** Generation of a Bessel beam by a reflective axicon.

Axicons based on reflection instead of refraction can be divided into positive on-axis axicons,[20] which never reached the market entry due to complicated optical setups and off-axis negative axicons (Fig. 2)[21] investigated in this paper. They provide improvements regarding damage threshold, chromatic aberrations, and group velocity dispersion compared to conventional axicons. Sophisticated measures to avoid heavy on-axis intensity oscillations become obsolete since the beam intensity profile in the propagation direction follows the smooth ideal curve closely.[21] Slight deviations come from the remaining surface error of <4 nm (RMS).

In the present work, we compare and analyze the spatial energy distribution of the Bessel beam generated by a reflective axicon with that of a conventional axicon experimentally and theoretically. Moreover, the capability to machine surface structures in the sub-$\mu$m range is demonstrated on copper samples.

## II. EXPERIMENTAL SETUP

The experiments were carried out in the facilities of the Fraunhofer ILT. The system is comprised of high-precision linear axes from Physik Instrumente (PI) and an ultrafast laser beam source from Edgewave. It provides a wavelength of $\lambda = 343$ nm, a maximum pulse energy of $E_P = 6\,\mu J$, a pulse repetition rate of $f_{rep} = 5$ MHz, and a pulse duration of $\tau = 400$ fs. Furthermore, a chromatic-confocal height measurement system for the adjustment of the focal distance and the detection of the tilt as well as an offset camera for lateral positioning are included in the system.

There are two optical setups realized on the motorized Z axis. The first one [Fig. 3(a)] generates the primary Bessel profile by reflection on the off-axis axicon Canunda from Cailabs with a base angle of $\alpha_{refl} = 1.14°$, while the second one [Fig. 3(b)] uses the conventional fused silica axicon AX125-A from Thorlabs with a refractive index of $n_{Ax} = 1.478$ and a base angle of $\alpha_{conv} = 5°$. The Gaussian beam radius ($1/e^2$) incident on the axicons amounts roughly 2 mm. In both setups, the primary Bessel profile is then demagnified by the same 4f-arrangement consisting of a plano-convex lens ($f_1 = 75$ mm @800 nm) and an asphere ($f_2 = 25$ mm@780 nm). The distance between these two lenses is experimentally determined to be 98 mm for the given wavelength in the UV. This telescope decreases the radial and axial Bessel core dimensions by the factor $f_1/f_2 = 3$ and $(f_1/f_2)^2 = 9$, respectively.[22] The generation of a smaller secondary Bessel profile is commonly preferred in material processing due to a higher energy density and a larger working distance.

A beam profiling unit [Fig. 3(c)] is mounted on the motorized XY Stage. It comprises a 15×microscope objective, a tube lens with a 400 mm focal length, an ND filter to exclude ambient light, and the CMOS camera Basler acA3800–14 $\mu$m for imaging. Images of the focal plane of the microscope objective are acquired along the

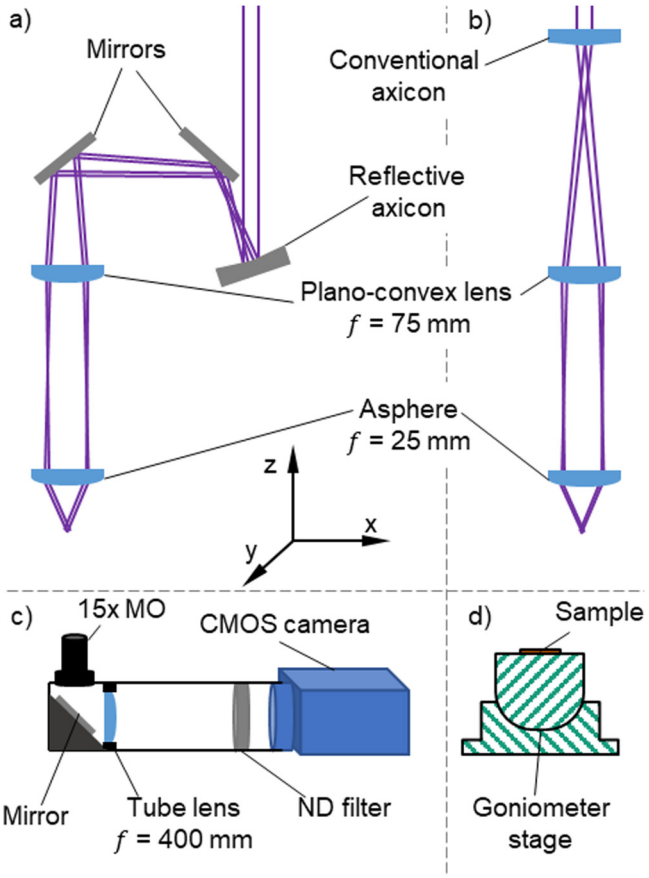


**FIG. 3.** Schematic of the experimental setups.

propagation axis, slice by slice by elevating the Z stage. For the ablation tests, the beam profiling unit is replaced by a polished copper sample of the size $40 \times 20 \times 3\ \text{mm}^3$ located on a compact goniometer stage [Fig. 3(d)]. The controller of the axis regulates the relative movement between the sample and the beam and triggers the laser accordingly.

## III. THEORETICAL ANALYSIS

In our simulation model, we consider the case where an axicon is illuminated by an ideal fundamental Gaussian beam with the waist $w_0$. Approximating the axicon (reflective or conventional) as a thin phase-only optical element and neglecting all phase terms that do not vary with the radial coordinate, we can write the electric field right behind the axicon as[23]

$$E(\rho, z = 0) = E_0 e^{-(\rho/w_0)^2} e^{ik\phi_{Ax}(\rho)}, \tag{1}$$

where $\phi_{Ax}$ accounts for the optical path difference introduced by the axicon and $k$ is the wavenumber. For the free-space propagation of this field, the rotational symmetry of the field allows us to use a 1D Hankel transform instead of the standard 2D Fourier transform based propagators and this can be expressed as

$$S(R, 0) = k \int E(\rho, 0)\rho J_0(kR\rho)d\rho, \tag{2}$$

where $R$ is the projection of the wavevector on the radial coordinate $\rho$.

The frequency spectrum at a distance $z$ is given by

$$S(R, z) = S(R, 0) \exp\left(ikz\left(\sqrt{1 - R^2}\right)\right). \tag{3}$$

Eventually, the field in the real space can be obtained by an inverse transform of $S(R,z)$.

### A. Conventional axicon

In order to model the optical path difference introduced by a conventional axicon with a round tip, we model the surface profile of the axicon as a hyperboloid of the form[6]

$$z_{hyp} = \sqrt{(a^2 + (\rho^2/\tan^2(\tau/2)))}, \tag{4}$$

where $\tau$ is the apex angle of the axicon and the parameter $a$ accounts for deviation of the round-tip axicon to that of an ideal axicon surface which is conical (illustrated in Fig. 4). This is related to the optical path difference $\phi_{Ax}$ as

$$\phi_{Ax}(\rho) = \Delta n z_{hyp}(\rho), \tag{5}$$

where $\Delta n$ denotes the difference between the axicon's and the ambient medium's refractive index.

In the case of the conventional axicon, we extract the needed values from fitting the experimentally measured depth profile (see Fig. 5) with the hyperboloid as described above, and we obtain the values for the parameter $a$ as $5.44 \pm 0.16\,\mu\text{m}$ and the base angle of the axicon $\alpha_{conv}$ as $4.78° \pm 0.09°$.

Please note the exceptional manufacture quality since the typical order of the parameter $a$ lies in the range of 30–50 $\mu$m.[4,6,15,17] The relay telescope that images the resulting Bessel beam is modeled via conventional ray optics, which account for the demagnification by a factor of 3 to mimic the experimental system.

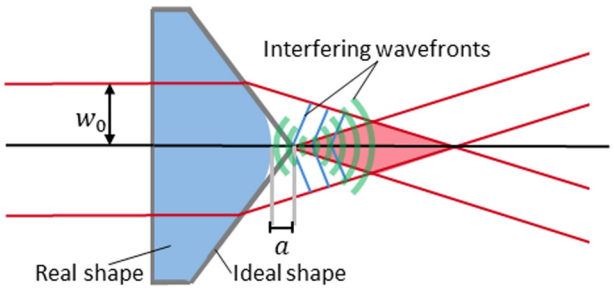


**FIG. 4.** Schematic of a round-tip axicon with the parameter $a$. The green wavefronts are caused by the round tip, while the blue wavefronts stem from the conical surface.

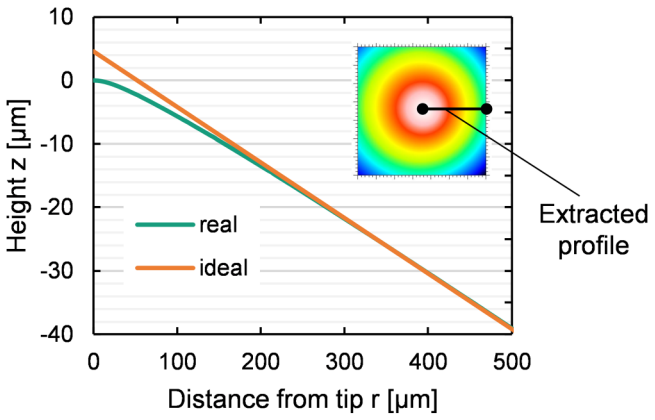


**FIG. 5.** White light interferometer measurement of the conventional axicon's tip deviation.

Figures 6 and 7 show the influence of the round tip at the incident beam waist of 2 and 1 mm ($1/e^2$), respectively. As expected, any deviation from the ideal axicon tip leads to oscillations in the beam and to an axial shift of the position of the beam peak intensity due to the lens effect.[18] Hence, using a larger beam on the axicon partially mitigates the effect of a marginally round-tip axicon. The use of larger beams will however lead to a lower energy density within the Bessel beam as the input energy is spread along the whole depth of field and will not suit some processes.

For a perfectly collimated beam of waist 2 mm and considering the demagnification introduced by the relay telescope, the resulting dimension for the Bessel core radius is $r_{B,sec} = 0.8\,\mu$m ($1/e^2$) and the Bessel zone length is $z_{B,sec} = 4.45$ mm (FWHM). As expected, the intensity peaks at a certain point and drops again.

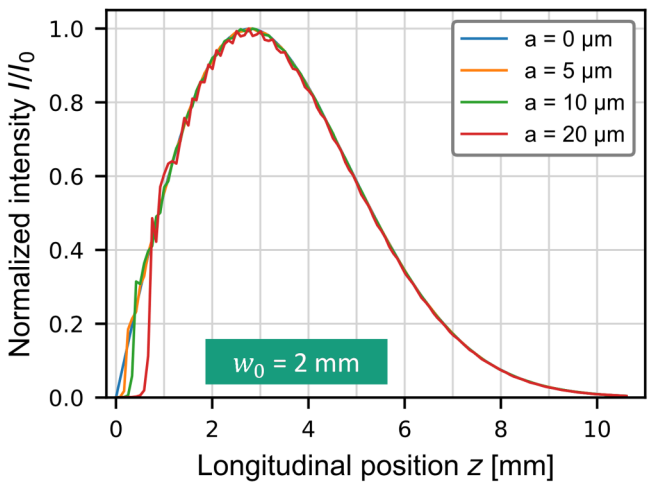


**FIG. 6.** Influence of a round tip on the generated on-axis intensity of the Bessel beam at an incident beam waist of $w_0 = 2$ mm.

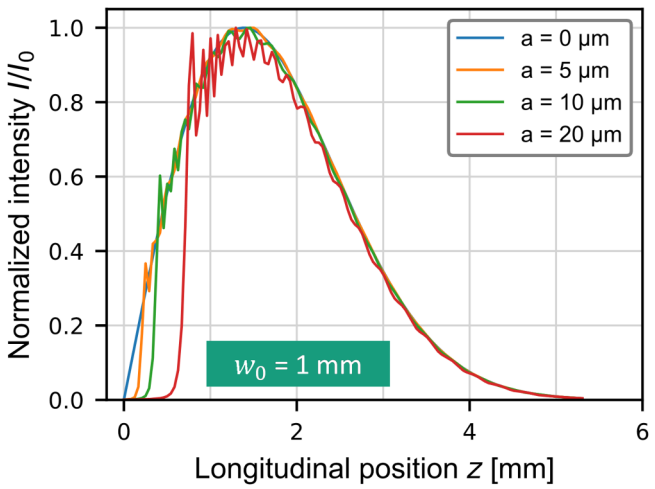


**FIG. 7.** Influence of a round tip on the generated on-axis intensity of the Bessel beam at an incident beam waist of $w_0 = 1$ mm.

### B. Reflective axicon

A less significant deviation from the ideal Bessel beam is assumed for the reflective axicon. The Bessel core radius depends on the deflection angle, which is $2\alpha_{refl}$. Formulas found in the literature for the conventional axicon can be easily converted by replacing $\alpha_{conv}(n_{Ax} - 1)$ with $2\alpha_{refl}$. The $1/e^2$ radius, which is commonly used in material processing, can be calculated using the small angle approximation as follows:

$$r_{B,pri} = \frac{1.75 \cdot \lambda}{2\pi \cdot 2\alpha_{refl}}. \tag{6}$$

The factor 1.75 is taken from the squared Bessel function $J_0^2$. It corresponds to the argument where the function value has dropped to $1/e^2$. For the given experimental setup, the Bessel core radii $r_{B,pri} = 2.4\,\mu$m and $r_{B,sec} = 0.8\,\mu$m are obtained.

The approximate Bessel zone length can be derived from a geometrical approach (see Fig. 2),

$$z_{B,pri} = \frac{w_0}{2\alpha_{refl}}. \tag{7}$$

With the parameters of the before mentioned experimental setup, the application of Eq. (7) results in a primary Bessel zone length of $z_{B,pri} = 29.6$ mm and a secondary Bessel zone length of $z_{B,sec} = 3.3$ mm after the demagnification.

## IV. EXPERIMENTAL RESULTS AND DISCUSSION

### A. Spatial intensity distribution

Figure 8 shows the colorized intensity plots of both kinds of axicons in transverse and longitudinal directions. As known from theory, the highest energy density is located in the central lobe, while the intensity of the concentric rings around it is very weak in

comparison. Nevertheless, there is the same energy on each ring, just distributed on different sized areas. In both cases, the high quality of the beam is evident, as well as the extremely high aspect ratio of the central lobe. The difference between the differently generated Bessel beams is less pronounced than expected from the literature due to the relatively sharp tip of the conventional axicon.

Because on-axis intensity is of particular interest for surface structuring, it is analyzed in more detail in the following. Figures 9 and 10 show the intensity data points with error bars for the reflective and conventional axicon, respectively. The data points are then fitted with the following function derived from[24]

$$I(z) = A \cdot z \cdot e^{-B \cdot z^2} + C. \tag{8}$$

This fit delivers the secondary Bessel zone length $z_{B,sec}$ as indirect output, while $A$, $B$, and $C$ are auxiliary constants. To be able to validate the measured intensity profile against actual ablation results, a line is marked every 25 $\mu$m in the z-direction with a pulse energy of around $E_P = 7$ nJ at a constant speed of 25 mm/s. The visual contrast of the marked lines matches the measured intensity profile quite well.

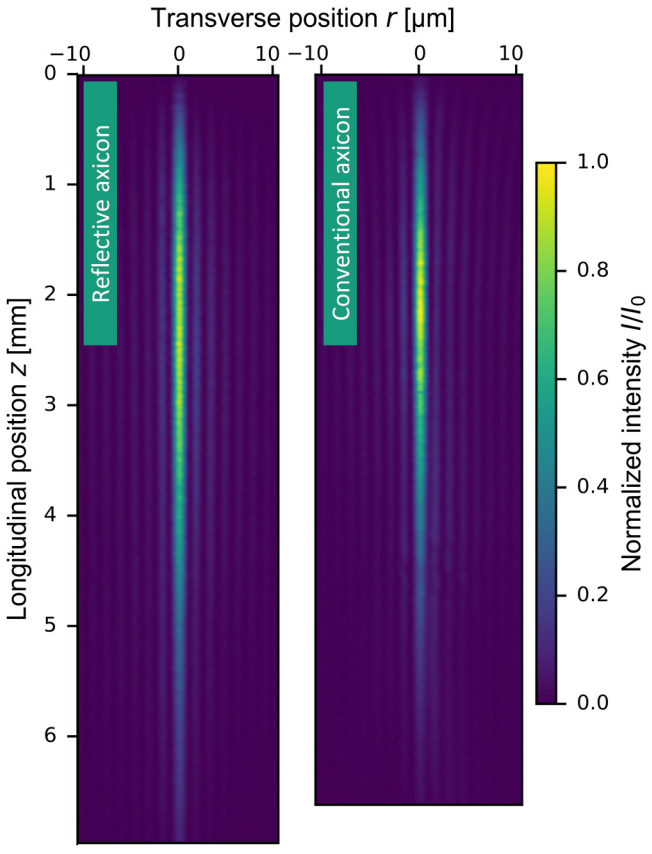


**FIG. 8.** Intensity distribution of the Bessel beams generated by the reflective and conventional axicons after demagnification.

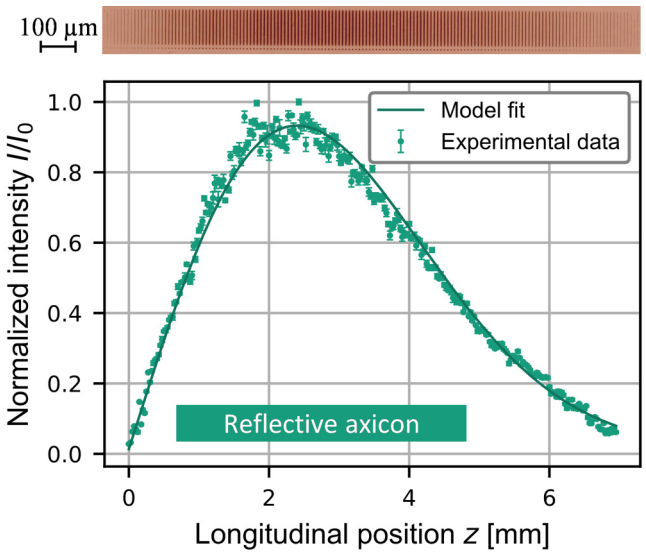


**FIG. 9.** Measured on-axis intensity evolution along the Bessel beam propagation for the reflective axicon and the corresponding ablation morphology on copper.

At first glance, it is obvious that the Bessel beam generated by the reflective axicon matches the ideal curve more closely. A slight oscillation can be observed for the conventional axicon. The model

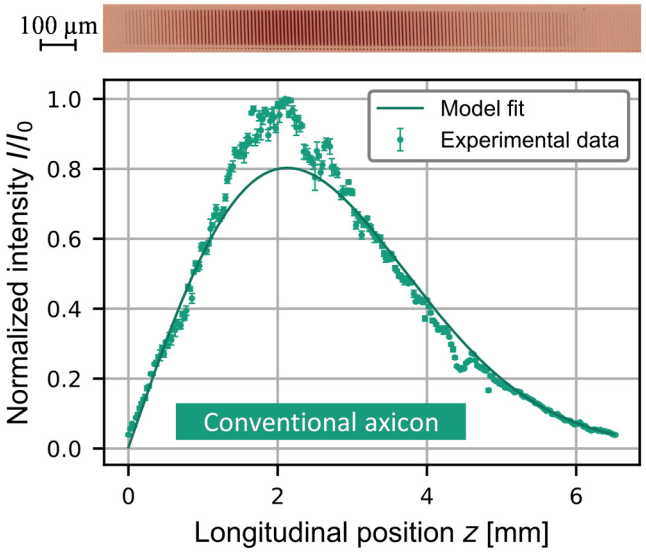


**FIG. 10.** Measured on-axis intensity evolution along the Bessel beam propagation for the conventional axicon and the corresponding ablation morphology on copper.

fit reveals a greater Bessel zone length $z_{B,sec}$ (FWHM) for the reflective axicon with 3.88 mm compared to 3.42 mm for the conventional axicon. Deviations from the theoretical results might stem from the assumed incident Gaussian beam radius or because the incident Gaussian beam is not perfectly collimated in the experiment.

In theory, the central core size stays constant in the longitudinal direction due to the nondiffracting nature of the Bessel beam. The experimental measurements (see Figs. 11 and 12) can confirm this behavior over a certain distance. However, the reflective axicon seems to generate a more constant radius than the conventional axicon, which seems to have a minimum at around $z = 2.5$ mm. Readings at the edges of the measurement range are not reliable because the transverse Bessel profile is too distorted, as can be seen in the exemplary intensity cross sections.

The Bessel core radius $r_{B,sec}$ of the reflective axicon is approximately 0.92 $\mu$m, while it amounts to 0.83 $\mu$m for the conventional radius. The experimental values slightly exceed the theoretical ones. Reasons for this, besides the divergent incident Gaussian beam, might be the limited beam quality $M^2$ or an error caused by the beam profiling unit.

### B. Surface structuring applications

The ability of the Bessel beam to structure in the submicrometer range is demonstrated by a simple crosshatch structure with a line pitch of 2 $\mu$m. The SEM image is shown in Fig. 13. The width of the ablated grooves is about 400 nm, which are significantly narrower than the $1/e^2$ diameter of the Bessel core of 1.8 $\mu$m. Such a behavior can be observed at fluences slightly above the threshold fluence.[25] The shallow material layer in the irregular zone around the narrow grooves is assumed to have been removed as a consequence of heat accumulation. Heat accumulation can only occur on highly thermal conductive materials like copper when the spatial and temporal pulse separation is very low. Both conditions are fulfilled in the experimental setup since the applied maximum velocity of the XY stage is $v = 300$ mm/s resulting in a distance between two consecutive pulses of only 0.06 $\mu$m at $f_{rep} = 5$ MHz. For comparison, a more adequate pulse spacing would be, e.g., 0.5 $\mu$m for this spot size.

The other experiment's scope is to demonstrate the enormous focal plane tolerance. For this purpose, the sample is tilted 5° by the goniometer stage. The test structure is 500 $\mu$m wide resulting in a

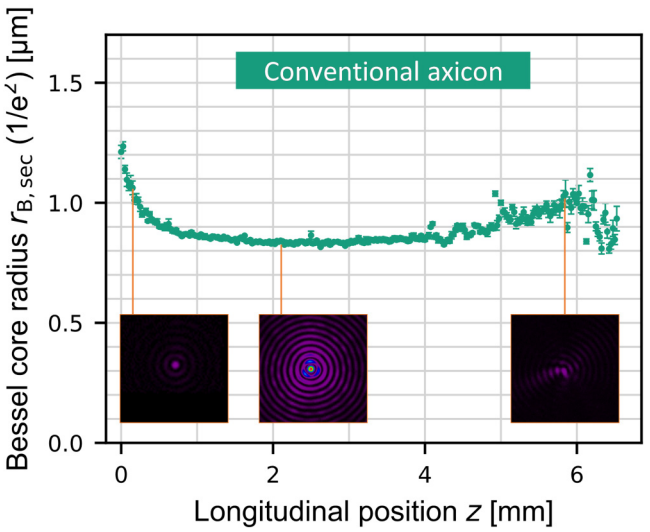


**FIG. 12.** Measured Bessel core radii along the beam propagation for the conventional axicon.

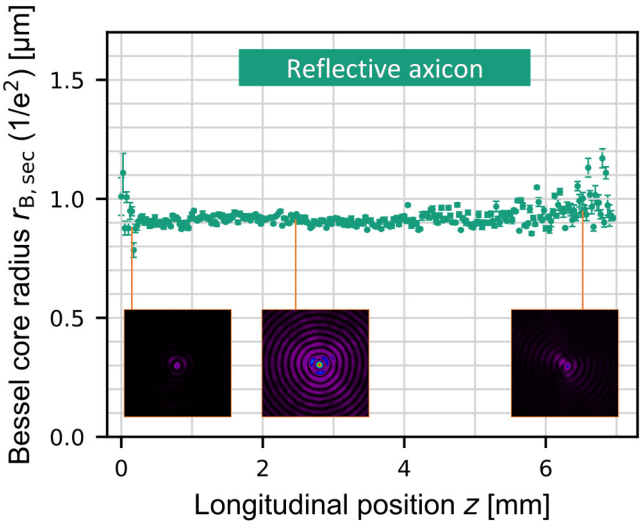


**FIG. 11.** Measured Bessel core radii along the beam propagation for the reflective axicon.

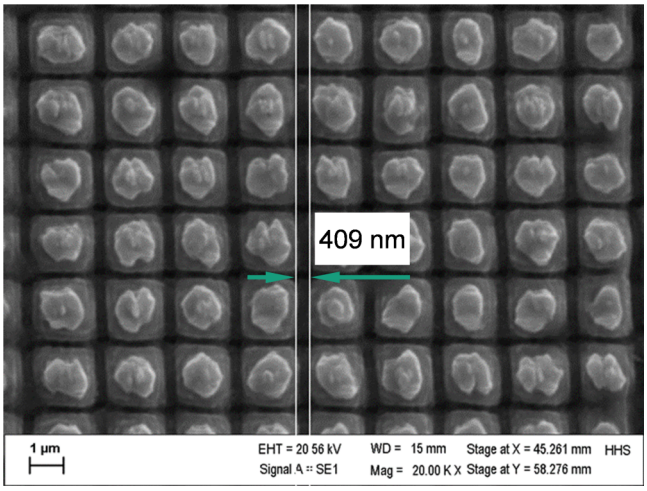


**FIG. 13.** SEM image of a crosshatch structure machined using the Bessel beam generated by the reflective axicon.

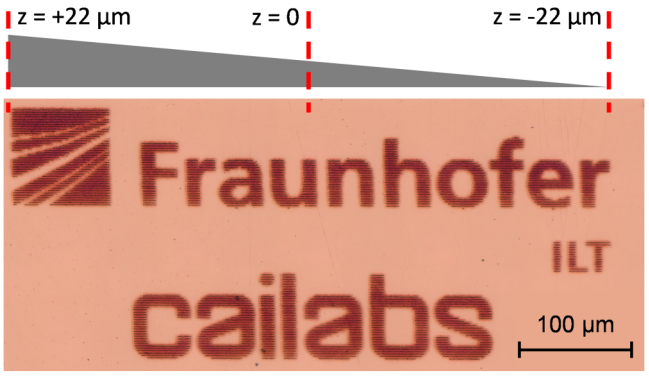


**FIG. 14.** Light microscope image of the ablated logos on a 5° tilted flat sample machined with the reflective axicon setup.

height variation over 44 $\mu$m from left to right. The structure is unidirectionally ablated from left to right using a pitch of 3 $\mu$m. Figure 14 shows the outcome of the experiment. No difference in the ablation result from left to right is observed. Thus, it is experimentally proven that submicrometer surface structuring using Bessel beams is suitable for highly challenging surface conditions.

## V. CONCLUSION

In this study, we showed that the use of Bessel beams in lieu of Gaussian beams is particularly suitable for USP laser surface structuring of feature sizes in the submicrometer regime due to their extremely high aspect ratio. Under favorable conditions, a Bessel beam generated by a reflective axicon does not differ greatly from one generated by a conventional axicon. This is the case when the input beam is relatively large and the axicon tip is very sharp. However, commercially available conventional axicons often do not have such sharp tips and the input beam is often kept small to maximize energy efficiency. In this case, the reflective axicon can provide a more stable surface structuring process due to lower intensity oscillations.

## ACKNOWLEDGMENT

This project was partially funded by the European Regional Development Fund (ERDF).

## REFERENCES

[1]J. Lopez, K. Mishchik, B. Chassagne, C. Javaux Leger, C. Hönninger, E. Mottay, and R. Kling, "Glass cutting using ultrashort pulsed Bessel beams," in *International Congress on Applications of Lasers & Electro-Optics* (Laser Institute of America, Atlanta, GA, 2015), pp. 60–69.
[2]M. Duocastella and C. B. Arnold, "Bessel and annular beams for materials processing," Laser Photonics Rev. **6**, 607–621 (2012).
[3]F. Courvoisier, J. Zhang, M. K. Bhuyan, M. Jacquot, and J. M. Dudley, "Applications of femtosecond Bessel beams to laser ablation," Appl. Phys. A **112**, 29–34 (2013).
[4]A. Michalowski, C. Freitag, R. Weber, and T. Graf, *Proc. SPIE* 7920, 79200W (2011).
[5]S. Kumar, S. M. Eaton, M. Bollani, B. Sotillo, A. Chiappini, M. Ferrari, R. Ramponi, P. Di Trapani, and O. Jedrkiewicz, "Laser surface structuring of diamond with ultrashort Bessel beams," Sci. Rep. **8**, 14021 (2018).
[6]O. Brzobohatý, T. Cizmár, and P. Zemánek, "High quality quasi-Bessel beam generated by round-tip axicon," Opt. Express **16**, 12688–12700 (2008).
[7]J. Durnin, J. J. Miceli, Jr., and J. H. Eberly, "Diffraction-free beams," Phys. Rev. Lett. **58**, 1499–1501 (1987).
[8]J. Turunen, A. Vasara, and A. T. Friberg, "Holographic generation of diffraction-free beams," Appl. Opt. **27**, 3959–3962 (1988).
[9]D. Flamm, D. Grossmann, M. Jenne, F. Zimmermann, J. Kleiner, M. Kaiser, J. Hellstern, C. Tillkorn, and M. Kumkar, *Proc. SPIE* 10904, 109041G (2019).
[10]J. Amako, K. Yoshimura, D. Sawaki, and T. Shimoda, Proc. SPIE **5713**, 497–507 (2005).
[11]A. Vasara, J. Turunen, and A. T. Friberg, "Realization of general nondiffracting beams with computer-generated holograms," J. Opt. Soc. Am. A **6**, 1748–1754 (1989).
[12]J. Leach, G. M. Gibson, M. J. Padgett, E. Esposito, G. McConnell, A. J. Wright, and J. M. Girkin, "Generation of achromatic Bessel beams using a compensated spatial light modulator," Opt. Express **14**, 5581–5587 (2006).
[13]J. H. McLeod, "Axicons and their uses," J. Opt. Soc. Am. **50**, 166–169 (1960).
[14]S. Schwarz, G.-L. Roth, S. Rung, C. Esen, and R. Hellmann, "Fabrication and evaluation of negative axicons for ultrashort pulsed laser applications," Opt. Express **28**, 26207–26217 (2020).
[15]J. Dudutis, P. GeČys, and G. Račiukaitis, "Non-ideal axicon-generated Bessel beam application for intra-volume glass modification," Opt. Express **24**, 28433–28443 (2016).
[16]X. Zeng and F. Wu, "Effect of elliptical manufacture error of an axicon on the diffraction-free beam patterns," Opt. Eng. **47**, 083401 (2008).
[17]P. Wu, C. Sui, and W. Huang, "Theoretical analysis of a quasi-Bessel beam for laser ablation," Photonics Res. **2**, 82–86 (2014).
[18]S. Akturk, B. Zhou, B. Pasquiou, M. Franco, and A. Mysyrowicz, "Intensity distribution around the focal regions of real axicons," Opt. Commun. **281**, 4240–4244 (2008).
[19]S. Akturk, C. L. Arnold, B. Prade, and A. Mysyrowicz, "Generation of high quality tunable Bessel beams using a liquid-immersion axicon," Opt. Commun. **282**, 3206–3209 (2009).
[20]W. R. Edmonds, "The reflaxicon, a new reflective optical element, and some applications," Appl. Opt. **12**, 1940–1945 (1973).
[21]P. Boucher, J. D. Hoyo, C. Billet, O. Pinel, G. Labroille, and F. Courvoisier, "Generation of high conical angle Bessel-Gauss beams with reflective axicons," Appl. Opt. **57**, 6725–6728 (2018).
[22]J. Dudutis, R. Stonys, G. Račiukaitis, and P. GeČys, "Aberration-controlled Bessel beam processing of glass," Opt. Express **26**, 3627–3637 (2018).
[23]Tomás Cizmár, "Optical traps generated by non-traditional beams," Ph.D. thesis, Masaryk University in Brno, 2006.
[24]C. Kalupka, *Energiedeposition von Ultrakurz Gepulster Laserstrahlung in Gläsern = Energy Deposition of Ultrashort Pulsed Laser Radiation in Glasses* (RWTH Aachen University, Germany, 2019).
[25]F. Korte, S. Adams, A. Egbert, C. Fallnich, A. Ostendorf, S. Nolte, M. Will, J. P. Ruske, B. Chichkov, and A. Tuennermann, "Sub-diffraction limited structuring of solid targets with femtosecond laser pulses," Opt. Express **7**, 41–49 (2000).

## Meet the Authors

Martin Osbild works as a project manager at the Fraunhofer Institute for Laser Technology (ILT) in Aachen, Germany. He is a member of the "Micro- and Nanostructuring" group. His research areas focus on ultrashort pulse laser applications, such as surface structuring and polishing. Among other topics, he analyzes the influence of beam shaping on surface structuring in the nanometer range.